*Journal of Biomolecular NMR*, **16:** 261–268, 2000.
*KLUWER/ESCOM*



# Inter- and intramolecular distance measurements by solid-state MAS NMR: Determination of gramicidin A channel dimer structure in hydrated phospholipid bilayers

Riqiang Fu[a], Myriam Cotten[a,b] & Timothy A. Cross[a,b,c,*]
[a]*Center for Interdisciplinary Magnetic Resonance, National High Magnetic Field Laboratory;* [b]*Department of Chemistry; and* [c]*Institute of Molecular Biophysics, Florida State University, Tallahassee, FL 32310, U.S.A.*

Received 15 September 1999; Accepted 24 January 2000

*Key words:* distance constraints, gramicidin A, simultaneous frequency and amplitude modulation, solid-state NMR

**Abstract**

Distance constraints are an important complement to orientational constraints. While a high-resolution monomer structure of the ion channel forming polypeptide, gramicidin A, has been solved with 120 orientational constraints, the precise geometry of the dimer interface has not been characterized. Here, using both $^{13}C$ and $^{15}N$ labeled gramicidin A samples in hydrated phospholipid bilayers, both inter- and intramolecular distances have been measured with a recently developed simultaneous frequency and amplitude modulation (SFAM) solid-state NMR scheme. Using this approach $^{15}N$-$^{13}C_1$ residual dipolar couplings across a hydrogen bond as small as $20 \pm 2$ Hz have been characterized. While such distances are on the order of $4.2 \pm 0.2$ Å, the spectroscopy is complicated by rapid global motion of the molecular structure about the bilayer normal and channel axis. Consequently, the nominal 40 Hz dipolar coupling is averaged depending on the orientation of the internuclear vector with respect to the motional axis. The intermolecular distance confirmed the previously described monomeric structure, while the intramolecular distance across the monomer–monomer interface defined this junction and confirmed the previous model of this interface.

## Introduction

Precise distance constraints are an important complement to orientational constraints for defining tertiary and quarternary protein structure. For gramicidin the monomeric structure is known to very high resolution through the extensive use of orientational constraints (Ketchem et al., 1993, 1997; Kovacs et al., 1999). However, the dimer interface is only modeled in a lipid environment since symmetry and the absolute nature of orientational constraints prevent the characterization of this junction. Distances represent relative constraints in that they restrict the position of one molecular site relative to another. Furthermore, distances are measured from through-space interactions and can be inter- or intramolecular. Consequently, the combined use of relative and absolute constraints is a powerful approach for characterizing this monomer–monomer junction.

Gramicidin A (gA), a major synthetic product of *Bacillus brevis*, is a polypeptide of 15 amino acid residues having the sequence of formyl-L-$Val_1$-$Gly_2$-L-$Ala_3$-D-$Leu_4$-L-$Ala_5$-D-$Val_6$-L-$Val_7$-D-$Val_8$-L-$Trp_9$-D-$Leu_{10}$-L-$Trp_{11}$-D-$Leu_{12}$-L-$Trp_{13}$-D-$Leu_{14}$-L-$Trp_{15}$-ethanolamine. All the alternating D- and L-amino acid side chains project on one side of the β-strand secondary structure, so as to force the strand to take on a helical conformation. In lipid bilayers, the polypeptide forms a monovalent cation selective channel that is dimeric, but single-stranded. The high-resolution structure of the channel monomer has been defined with 120 precise orientational constraints from solid-state NMR of uniformly aligned samples in lipid

*To whom correspondence should be addressed. E-mail: cross@magnet.fsu.edu

bilayers (Ketchem et al., 1993, 1996, 1997; Kovacs et al., 1999). It features a single-stranded helix with a right-handed sense, 6.5 residues per turn, and β-strand torsion angles. The monomer–monomer geometry (amino terminal to amino terminal) has been characterized by solution NMR in sodium dodecyl sulfate (SDS) micelles (Lomize et al., 1992) in which the monomer fold proved to be the same as in lipid bilayers. However, no direct evidence of the monomer–monomer geometry has yet been obtained in lipid bilayers, although models for the monomer–monomer junction were characterized through the combined studies of conductance and chemical modifications (Bamberg and Lauger, 1973; O'Connell et al., 1990; Tian and Cross, 1999). The intermonomer distance measurements generated here provide a straightforward approach for characterizing the dimeric structure of gA in lipid bilayers.

In this paper, specifically $^{13}C/^{15}N$ spin pairs are incorporated into gA in hydrated phospholipid bilayers so that the intermonomer and intramonomer distances can be obtained from modest residual dipolar couplings using a recently developed simultaneous frequency and amplitude modulation (SFAM) (Fu et al., 1997) technique which allows for measurements of extremely weak residual dipolar couplings. The measured intramonomer distances confirm the validity of the approach while the intermonomer distances lead to a determination of the dimeric channel structure.

## Materials and experiments

Gramicidin A (gA) was synthesized by solid phase peptide synthesis using Fmoc (9-fluorenylmethoxycarbonyl) chemistry on an Applied Biosystems model 430A peptide synthesizer. The blocking chemistry of isotopically labeled amino acids (Cambridge Isotope Laboratories, Woburn, MA) was performed in our laboratory. Details of the synthesis and blocking chemistry have been described previously (Fields et al., 1988, 1989).

After synthesis and cleavage from the solid phase support, the peptides were characterized and the purity was assessed. The protocol for characterization by HPLC has been previously described (Fields et al., 1989). Typical purity was greater than 98% and peptides were used without further purification.

Unoriented samples for solid-state NMR were prepared by codissolving gA and dimyristoylphosphatidylcholine (DMPC) in a 1:8 molar ratio in 95/5 (v/v) benzene/ethanol solution. After lyophilization, the white powder was hydrated through adding 50% HPLC-grade water (by total sample dry weight). The tubes were then sealed and incubated at 45 °C for a minimum of two weeks until the samples became uniformly hydrated. Before conducting the NMR experiments, the samples were transferred to a glass tube (Wilmad, Buena, NJ) designed to fit the NMR rotors. Epoxy glue was used to make a tight seal at the end of the glass tube.

Figure 1 shows the SFAM scheme and pulse sequence for the SFAM dipolar recoupling scheme. After enhancement by cross polarization, the $^{13}C$ magnetization evolves during two intervals separated by a 180° pulse, and then the $^{13}C$ signals are recorded at the echo time. A 180° $^{15}N$ pulse is also applied between the intervals in order to accumulate the dipolar dephasing. When the SFAM irradiation is applied to the $^{15}N$ spins during the intervals, the observed $^{13}C$ signals dephase due to the recovered $^{13}C$-$^{15}N$ dipolar interaction. As in the REDOR experiments (Gullion and Schaefer, 1989), the $^{13}C$ resonance intensities are monitored as a function of the rotor cycles with and without the SFAM irradiation on the $^{15}N$ spins. The difference ($\Delta S$) between two intensities depends exclusively on the dipolar interaction, thus yielding the internuclear distance between the $^{13}C$ and $^{15}N$ spins.

The distance measurements in hydrated unoriented samples were implemented on a Bruker DMX-300 NMR spectrometer ($B_0 = 7$ T), equipped with a Bruker CPMAS triple resonance probe with 7 mm rotors and with Larmor frequencies of 75 MHz for $^{13}C$, 30 MHz for $^{15}N$, and 300 MHz for $^{1}H$. In the experiments, a 2 kHz sample spinning rate was used in order to completely suppress the residual $^{13}C$ chemical shift anisotropy. The stability of the spinning rate was controlled within ±2 Hz by a Bruker pneumatic MAS unit. The parameters used for SFAM in our experiments included a modulation frequency of 2 kHz (equal to the spinning rate); the depth of the frequency modulation was 30 kHz. The maximum of the RF amplitude was set to 25 kHz. The waveforms for the amplitude and frequency modulation were generated by a C program and transferred to the waveform generator of the NMR console. The 180° pulse length was 16.8 μs for both $^{15}N$ and $^{13}C$. All spectra were recorded using cross polarization (5 μs 90° pulse length and 700 μs contact time) at a temperature of 315 K (above the gel-to-liquid crystalline phase transition temperature of the lipids). A recycle delay of 4 s was used and conventional high power continuous-

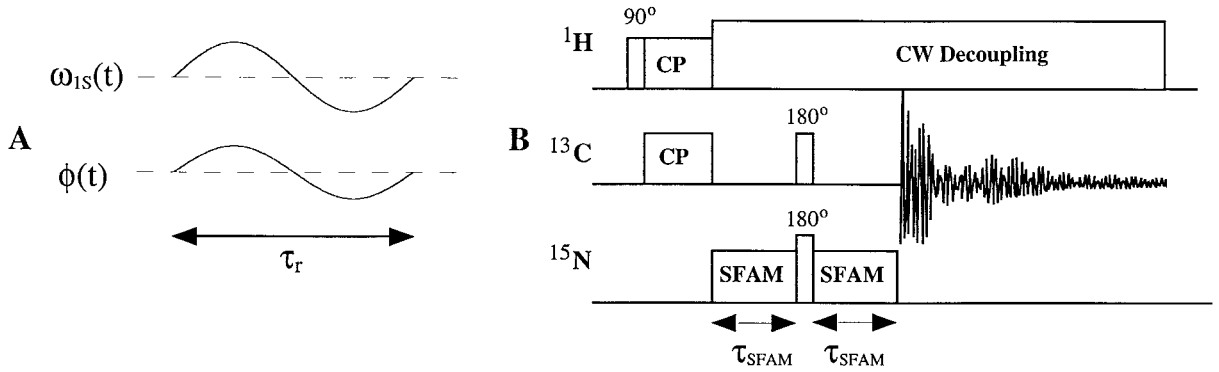


*Figure 1.* (A) Waveform of the simultaneous frequency and amplitude modulation (SFAM) for one rotor cycle, where $\omega_{1S}(t) = \omega_{1S}^{\max} \sin \omega_r t$ and $\phi(t) = \omega_\Delta \sin \omega_r t/\omega_r$ are the time-dependences of the amplitude and the instantaneous phase, respectively, $\tau_r = 2\pi/\omega_r$ is the sample rotational period, and $\omega_\Delta$ and $\omega_{1S}^{\max}$ stand for the depth of the frequency modulation and maximum RF amplitude, respectively. (B) Pulse sequence for the SFAM dipolar recoupling scheme, where the SFAM irradiation period $\tau_{SFAM}$ is applied before and after the 180° pulse on the $^{15}$N spins with an increment of multiples of the rotor cycle, i.e. $\tau_{SFAM} = N\tau_r$ with integer N, resulting in a total dipolar dephasing time of $2\tau_{SFAM}$.

wave proton decoupling was applied throughout the evolution and observation of the $^{13}$C magnetization. All simulations with the above SFAM parameters were carried out on the GAMMA magnetic resonance simulation platform (Smith et al., 1994).

## Results and discussion

In systems that undergo fast molecular motions, nuclear dipolar couplings are usually scaled by the molecular motions, resulting in weaker couplings. For gramicidin A in lipid bilayers above the gel-to-liquid crystalline phase transition, the global motion around the helical axis (i.e. bilayer normal) of the channel is on the microsecond time scale (North and Cross, 1995). Such a fast global motion will scale the nuclear dipolar coupling:

$$D_{obs} = D\frac{1}{2}(3\cos^2\theta - 1), \quad (1)$$

where $D_{obs}$ is the motionally averaged residual dipolar coupling that is to be observed experimentally, $D = \gamma_H\gamma_C h/2\pi r^3$ is the static internuclear dipolar coupling dependent on $r$, the internuclear distance, $\theta$, the orientation of the internuclear vector with respect to the motional axis, and $\gamma_H$ and $\gamma_C$ are the gyromagnetic ratios for $^1$H and $^{13}$C, respectively. The orientation results in a scaling factor of $(3\cos^2\theta - 1)/2$. At the magic angle (i.e. $\theta = 54.7°$), the scaling factor becomes zero; thereby no residual dipolar coupling can be observed.

Several factors should be considered before performing distance measurements in such samples. The first is the choice of the isotopically labeled pair in terms of spectroscopic preferences such as detectability and sensitivity of the nuclei. The backbone of gA is composed of C, N, and O elements. $^{17}$O is not a good choice because it is a low sensitivity quadrupolar nucleus. A $^{15}$N-$^{15}$N spin pair is also excluded due to the weak dipolar couplings resulting from both the relatively long distance and the low gyromagnetic ratio. A $^{13}$C-$^{13}$C pair may be attractive because it possesses a much larger dipolar coupling than a $^{15}$N-$^{15}$N pair for the same internuclear distance. Unfortunately, such labels have several disadvantages from the spectroscopic point of view. The isotropic chemical shifts of the carbonyl carbons have a very small chemical shift range, thereby making the distance measurement between two carbonyl carbons extremely difficult, while the α-carbons of the polypeptide are buried by the $^{13}$C background signals resulting from the lipid bilayers (Tian et al., 1999). Overall, a $^{13}$C/$^{15}$N pair between carbonyl carbon and amide $^{15}$N sites is the best choice in terms of spectroscopic preferences.

Secondly, the orientation of the internuclear vector of interest with respect to the global motional axis (equivalent to the channel axis) needs to be examined from the structural models. Fortunately, the three-dimensional high-resolution structure of gA in lipid bilayers has been defined by solid-state NMR-derived orientational constraints (Ketchem et al., 1997). Therefore, unfavorable orientations in the vicinity of the magic angle (i.e. 54.7°) can be easily avoided.

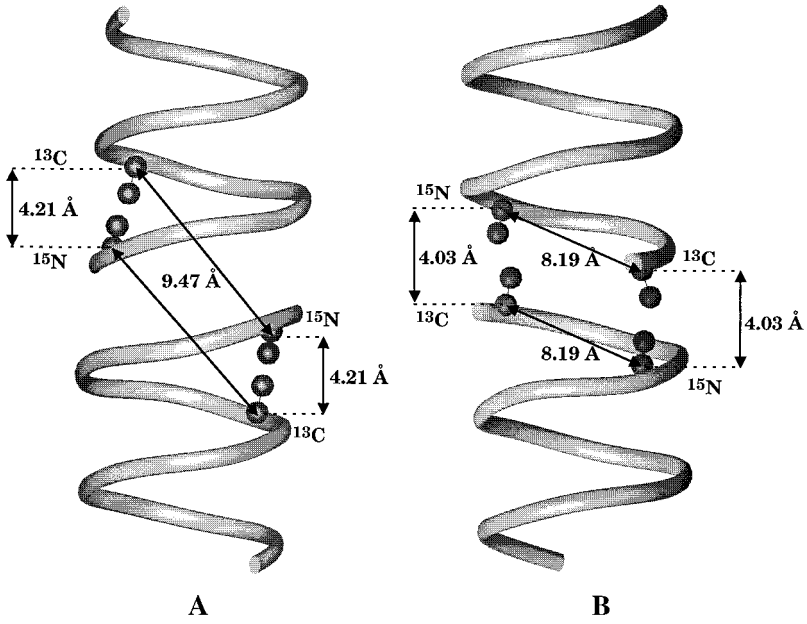


*Figure 2.* Positions of the specifically labeled $^{13}C$ and $^{15}N$ sites in gramicidin A observed in hydrated phospholipid bilayers. Both $^{13}C$ and $^{15}N$ labels are indicated by solid balls at the ribbon. The solid balls, away from the ribbon, but linked to the $^{13}C$ and $^{15}N$ labels, represent the oxygen and the hydrogen nuclei, respectively, which are favorably oriented for hydrogen bonding. The distances indicated in the figures are derived from the coordinates of the high-resolution gA structure (Ketchem et al., 1997) (PDB accession no. #1MAG). (A) $^{13}C_1$-Val$_7$, $^{15}$N-Gly$_2$ gA. For these labels, the distance between the intramonomer $^{13}C$ and $^{15}N$ sites is 4.21 Å, while the intermonomer $^{13}C$ and $^{15}N$ sites are 9.47 Å apart. (B) $^{13}C_1$-Val$_1$, $^{15}$N-Ala$_5$ gA. In this case, the separation between the intramonomer $^{13}C$ and $^{15}N$ sites is 8.19 Å, while the intermonomer $^{13}C$ and $^{15}N$ sites are modeled to be 4.03 Å apart, across the monomer–monomer junction.

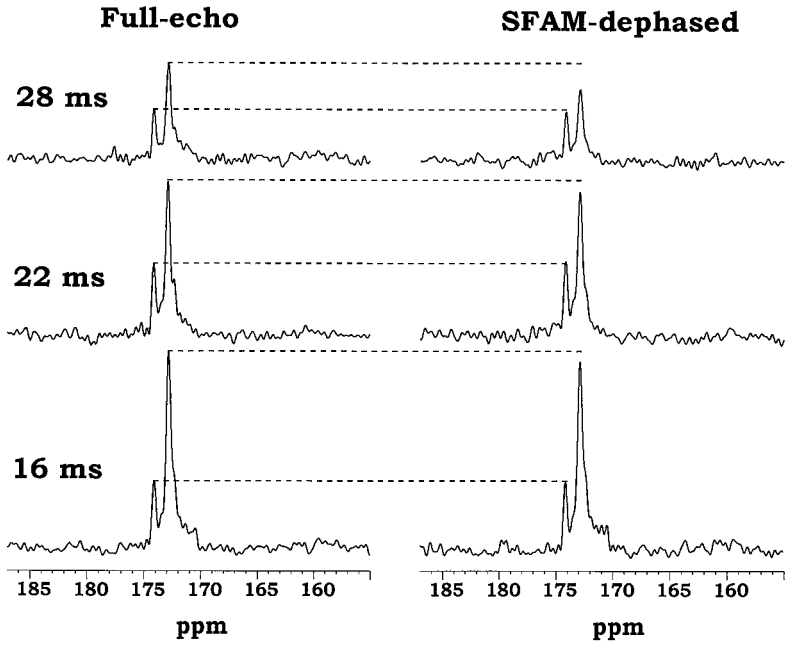


*Figure 3.* Sets of SFAM spectra of $^{13}C_1$-Val$_7$, $^{15}$N-Gly$_2$ gA in unoriented hydrated DMPC bilayers recorded at 315 K (above the gel-to-liquid crystalline phase transition temperature of the lipids) with (right) and without (left) various SFAM dephasing times. The horizontal dashed lines indicate the intensity differences between the two sets of spectra. The peak at 174.0 ppm is not affected by dephasing and is therefore assigned to the carbonyl group of the lipids. The peptide resonance at 172.8 ppm is dephased by the SFAM irradiation on the $^{15}N$ spins. For each spectrum 2048 scans were used for signal accumulation.

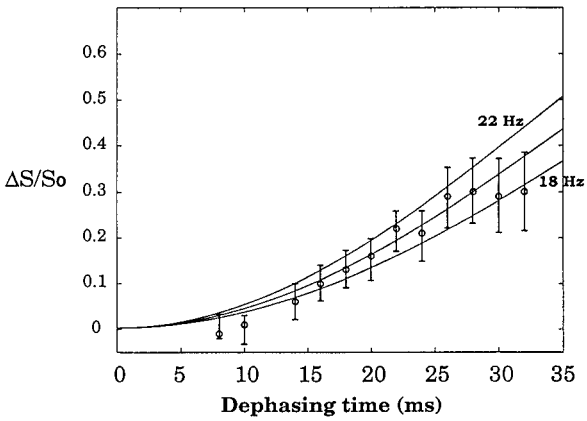


*Figure 4.* Plots of the ratio of SFAM difference (ΔS) to full-echo ($S_0$) intensities of the $^{13}C$ peptide resonance from the SFAM spectra of $^{13}C_1$-Val$_7$, $^{15}$N-Gly$_2$ gA shown in Figure 3 versus dephasing time. The experimental data (open circles) with error bars, which were calculated by considering the noise levels in the spectra, are compared to the curves simulated for dipolar couplings varying from 18 to 22 Hz in increments of 2 Hz. The average dipolar interaction between these labels is 20 ± 2 Hz, corresponding to a motionally averaged distance of 4.2 ± 0.2 Å.

Figure 2 presents two choices for specific $^{13}C/^{15}N$ isotopic labeling of gA. The $^{13}C$ and $^{15}N$ labels are incorporated into each monomer, but in different sites. Figure 2A shows a model of $^{13}C_1$-Val$_7$, $^{15}$N-Gly$_2$ gA. Based on the high-resolution monomer structure (Ketchem et al., 1997), the intramonomer distance is 4.21 Å and the orientation of the internuclear vector with respect to the motional axis is 35.3°, yielding a scaling factor of 0.5 for the dipolar interaction. The intermonomer distance between these $^{13}C/^{15}N$ labels is 9.47 Å, too long to yield a detectable dipolar coupling, based on the model of the amino terminal to amino terminal hydrogen-bonded single stranded dimer. In the $^{13}C_1$-Val$_1$, $^{15}$N-Ala$_5$ gA sample (Figure 2B), the intramonomer distance is 8.19 Å with a scaling factor of 0.36, resulting from an orientation of 40.9° with respect to the global motion axis. Such a dipolar coupling is too weak to be detectable. On the other hand, the intermonomer distance between the labels is 4.03 Å with an angle of 2.2° between the internuclear vector and the motional axis. The scaling factor resulting from this small angle is negligible, 0.997. Such a distance constraint should be observable. Therefore, whether or not the distance constraint between these two sites is detectable will directly confirm the modeled dimeric structure of gA in lipid bilayers.

Figure 3 shows the $^{13}C$ NMR spectra of the $^{13}C_1$-Val$_7$, $^{15}$N-Gly$_2$ gA in unoriented hydrated DMPC bilayers, with (right) and without (left) the SFAM irradiation on the $^{15}N$ spins. Only the carbonyl carbon signals are shown in the spectra. As indicated by the horizontal dashed lines, the resonance at 174.0 ppm is not affected by the SFAM irradiation and thus assigned to the natural abundance carbonyl groups of the lipids. The peptide resonance at 172.8 ppm is clearly dephased with the SFAM irradiation to the $^{15}N$ spins, indicating that the residual dipolar coupling between the labeled $^{13}C$ and $^{15}N$ sites exists. Figure 4 shows the plot of the ratio of the dephased intensity (ΔS) resulting from the SFAM irradiation to the full-echo intensity of the peptide $^{13}C$ resonance at 172.8 ppm versus dephasing time. By comparing the experimental data (open circles) with the simulated curves (solid lines) for the dipolar couplings between 18 and 22 Hz, a motionally averaged residual dipolar coupling, $D_{obs}$, of 20 ± 2 Hz was obtained. By taking into account the angle between the internuclear vector and the motional axis, which gives a scaling factor of 0.5, the dipolar coupling, $D$, of 40 ± 4 Hz between the $^{13}C$ and $^{15}N$ labels was calculated, implying a distance of 4.2 ± 0.2 Å between the labeled sites. This result is in good agreement with the one calculated from the high-resolution structure of the monomer (Ketchem et al., 1997). The result here proves that SFAM has great potential for measuring weak dipolar coupling (as small as 20 Hz) and illustrates the significant advantages of combining different types of constraints. The motionally averaged residual dipolar coupling may be used to characterize the orientation of the internuclear vector with respect to the motional axis if the magnitude of the dipolar coupling can be determined independently (Hing and Schaefer, 1993), or to determine the dipolar coupling if the orientation of the internuclear vector with respect to the motional axis can be obtained in separate experiments (Cotten et al., 1999).

Figure 5 shows the $^{13}C$ NMR spectra of $^{13}C_1$-Val$_1$, $^{15}$N-Ala$_5$ gA in unoriented hydrated DMPC bilayers, with (right) and without (left) the SFAM irradiation on the $^{15}N$ spins. As in Figure 3, only the carbonyl carbon signals are shown in the spectra; however, three peaks are visible. The $^{13}C$ resonance at 174.0 ppm does not dephase when applying the SFAM irradiation to the $^{15}N$ spins and thus can be assigned to the carbonyl groups of the lipids, as in Figure 3. Indeed, this lipid signal is at the same frequency as in the $^{13}C_1$-Val$_7$ gA (Figure 3), confirming its assignment. The remaining two resonances at 171.0 and 172.6 ppm are both dephased by the SFAM irradiation on the $^{15}N$ spins, implying that both $^{13}C$ resonances result from the $^{13}C_1$-Val$_1$ labeling (vide infra) and are dipolarly

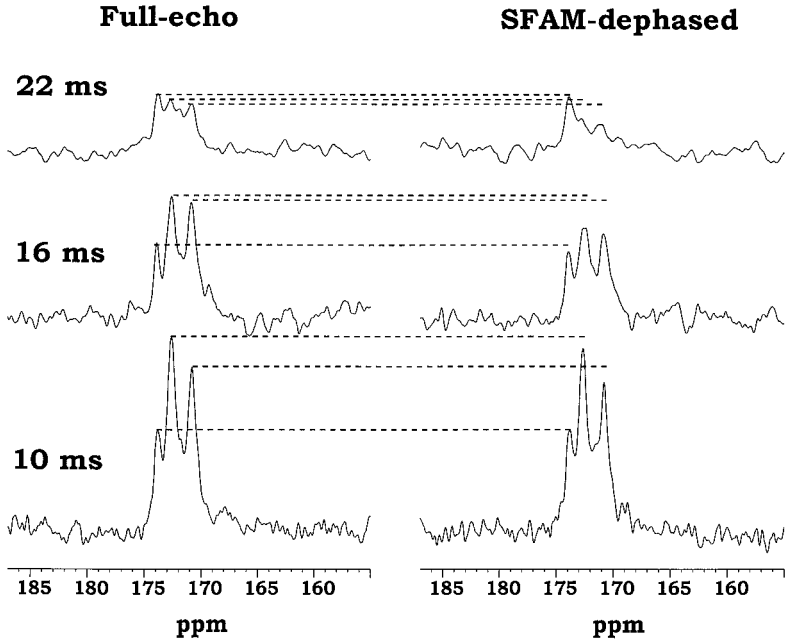


*Figure 5.* Sets of SFAM spectra of $^{13}C_1$-Val$_1$, $^{15}$N-Ala$_5$ gA in unoriented hydrated DMPC bilayers recorded at 315 K (above the gel-to-liquid crystalline phase transition temperature of the lipids) with (right) and without (left) various SFAM dephasing times. The horizontal dashed lines indicate the intensity differences between the two sets of spectra. Because the peak at 174.0 ppm is not dephased, it is therefore assigned to the carbonyl group of the lipids. The remaining two resonances at 171.0 and 172.6 ppm are dephased by the SFAM irradiation on the $^{15}$N spins. For longer dephasing times (e.g. 22 ms), more scans were taken for signal accumulation.

coupled with the labeled $^{15}$N site. The ratios of the dephased intensities ($\Delta$S) to the full-echo intensities for both resonances versus dephasing time are shown in Figure 6. It is clearly seen that both resonances have the same dephasing rate. The results imply that there are two $^{13}C_1$-Val$_1$ sites with different chemical environments having the same residual dipolar couplings with a single labeled $^{15}$N-Ala$_5$ site.

The two $^{13}$C isotropic resonances from the peptide have roughly the same intensity and about half the intensity of $^{13}C_1$-Val$_7$ in Figure 3 relative to the lipid carbonyl intensity. In addition, the two resonances appear at positions different from that for the $^{13}C_1$-Val$_7$ gA, implying that the two resonances are indeed from the $^{13}C_1$-Val$_1$ label rather than from the overlap of natural abundance carbonyl signals of the peptide. Repetition of the synthesis with great care to avoid racemization did not change the $^{13}$C spectra. Furthermore, HPLC sensitive to D versus L stereoisomers showed no indication of D-Val. Therefore, we conclude that the two isotropic signals arise from two conformations. However, these conformations must give rise to the same orientational constraints since no splitting of the orientational constraints have been

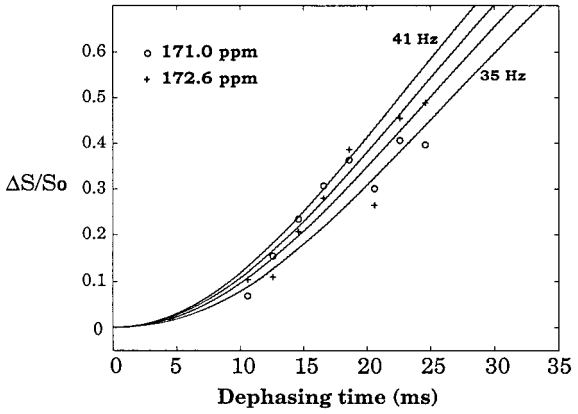


*Figure 6.* The signal intensities of $^{13}C_1$-Val$_1$, $^{15}$N-Ala$_5$ gA from the spectra in Figure 5 are used to graph the ratio of SFAM difference ($\Delta$S) to full-echo ($S_0$) intensities versus dephasing time. The experimental data for both resonances at 171.0 ppm (open circles) and at 172.6 ppm (crosses) are compared to the curves simulated for dipolar couplings varying from 35 to 41 Hz in increments of 2 Hz. The average dipolar interaction between these labels is $38 \pm 3$ Hz, corresponding to a motionally averaged distance of $4.3 \pm 0.1$ Å.

observed. Figure 7 illustrates a possible explanation for these two isotropic resonances that involves the existence of two different orientations for the Val$_1$ C=O

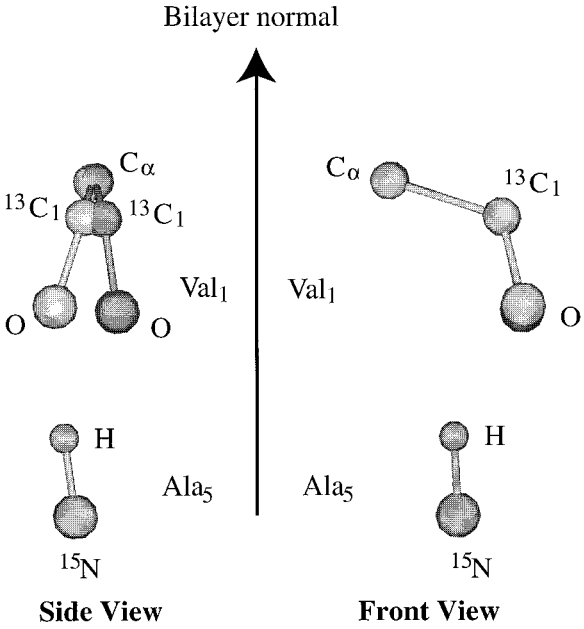


*Figure 7.* Two possible orientations of the intermolecular hydrogen bond between the oxygen of the $Val_1$ carbonyl group and the hydrogen of the N-H bond of $Ala_5$ from the initial structures derived solely from the NMR data and an assumed covalent geometry (Ketchem et al., 1996; Quine et al., 1997). The two peptide planes are well aligned, showing two different orientations in the side view (left) where the channel axis parallel to the lipid bilayer normal lies on the right side. When the structures are rotated around the channel axis by 90° the peptide planes are overlapped, as seen in the front view (right) whereby the channel axis is behind the figure. The different carbonyl orientations may result in different $^{13}C_1$ isotropic chemical shifts for the $Val_1$ residue while preserving the same distance between the $^{13}C_1$ and $^{15}N$ sites.

bond with respect to the channel axis. One of them has the C=O bond oriented slightly *towards* the channel axis while the other has it oriented slightly *away* from the channel axis. Since the channel axis is aqueous and the channel exterior is hydrophobic, different orientations may change the chemical environment, thereby resulting in different $^{13}C_1$ isotropic chemical shifts for the $Val_1$ residue while keeping the same intermonomer distance between the $^{13}C_1$ and $^{15}N$ labels as shown in the figure. The $Ala_5$ $^{15}N$-$^{1}H$ is known to be approximately parallel to the bilayer normal, as indicated by a dipolar coupling of 20.7 kHz, nearly a maximum dipolar coupling for the $^{15}N$-$^{1}H$ bond. Moreover, in the refinement performed by Ketchem and co-workers (Ketchem et al., 1997), two different orientations for the C=O bond of the $Val_1$ residue were consistent with the NMR-derived orientational constraints and the global energy of the structure. One of these orientations is about 10° towards the channel axis and the other one is about 20° away from the channel axis. These hypothesized conformational states at the monomer–monomer junction may be functionally important. Potentially, dynamic fluctuations between these states could account for channel flicker (Seoh and Busath, 1993) or open channel conductance noise (Heinemann and Sigworth, 1990).

By comparing the experimental data with the simulated curves for the dipolar couplings from 35 to 41 Hz, the motionally averaged residual dipolar couplings were determined to be 38 ± 3 Hz for both resonances. The motionally averaged dipolar couplings correspond to a distance of 4.3 ±0.1 Å. This distance suggests that, irrespective of the conformational ambiguity obtained above, the $Val_1$ C=O and $Ala_5$ N-H are hydrogen-bonded across the monomer–monomer junction. This result agrees well with the gA dimeric structure in SDS micelles (Lomize et al., 1992) in which six intermonomer hydrogen bonds involving the $Val_1$, $Ala_3$ and $Ala_5$ residues are formed to stabilize the dimeric channel structure.

## Conclusions

Distance constraints have been obtained here from unoriented hydrated lipid bilayer samples under MAS conditions using the recently developed SFAM technique (Fu et al., 1997). Residual dipolar couplings, as weak as 20 Hz, have been obtained from motionally averaged interactions. In addition, it has been shown that the $^{13}C/^{15}N$ labels are suitable for distance measurements in lipid bilayer samples, despite strong background $^{13}C$ signals. By incorporating $^{13}C_1$-$Val_7$ and $^{15}N$-$Gly_2$ labels into gA, an intramonomer dipolar coupling was obtained confirming the high-resolution structure in this bilayer environment (Ketchem et al., 1997). When incorporating the $^{13}C_1$-$Val_1$ and $^{15}N$-$Ala_5$ labels into gA, only the intermonomer dipolar coupling was observable, allowing for the characterization of the monomer–monomer junction in this lipid environment for the first time. Finally, magic angle spinning yields much higher resolution solid-state NMR spectra, which allow for the observation of different $^{13}C_1$ isotropic chemical shifts of the $Val_1$ residue. This observation suggests the existence of two local conformational states at the monomer–monomer junction that may be associated with channel function (Heinemann and Sigworth, 1990; Seoh and Busath, 1993).

It has also been demonstrated here that the combined use of orientational and distance constraints is a powerful structural approach. In fact, various types of constraints are synergistic. For instance, orientational and torsional constraints can determine the relative orientation of molecular groups, but neither of them is appropriate for precisely defining the separation of these groups, a task directly solved by distance constraints. Conversely, even precise distance measurements may leave the relative orientation of groups poorly defined. Therefore, the combination of these constraints has great utility in characterizing structures of protein and polypeptides, particularly in studies of tertiary and quarternary protein structure.

## Acknowledgements

The authors are indebted to H. Hendricks and U. Goli of the Bioanalytical Synthesis and Services, for their expertise and maintenance of the ABI 430A peptide synthesizer and HPLC equipment.

This work has been supported by the National Institutes of Health grant AI-23007 to T.A.C. and the work was largely performed at the National High Magnetic Field Laboratory supported by the National Science Foundation Cooperative Agreement DMR-9527035 and the State of Florida.

## References

Bamberg, E. and Lauger, P. (1973) *J. Membr. Biol.*, **11**, 177–194.
Cotten, M., Fu, R. and Cross, T.A. (1999) *Biophys. J.*, **76**, 1179–1189.
Fields, C.G., Fields, G.B., Boble, R.L. and Cross, T.A. (1989) *Int. J. Pept. Protein Res.*, **33**, 298–303.
Fields, G.B., Fields, C.G., Petefish, J., van Wart, H.E. and Cross, T.A. (1988) *Proc. Natl. Acad. Sci. USA*, **85**, 1384–1388.
Fu, R., Smith, S.A. and Bodenhausen, G. (1997) *Chem. Phys. Lett.*, **272**, 361–369.
Gullion, T. and Schaefer, J. (1989) *J. Magn. Reson.*, **81**, 196–200.
Heinemann, S.H. and Sigworth, F.J. (1990) *Biophys. J.*, **57**, 499–514.
Hing, A.W. and Schaefer, J. (1993) *Biochemistry*, **32**, 7593–7604.
Ketchem, R., Hu, W. and Cross, T.A. (1993) *Science*, **261**, 1457–1460.
Ketchem, R.R., Lee, K.-C., Huo, S. and Cross, T.A. (1996) *J. Biomol. NMR*, **8**, 1–14.
Ketchem, R.R., Roux, B. and Cross, T.A. (1997) *Structure*, **5**, 1655–1669.
Kovacs, F., Quine, J. and Cross, T.A. (1999) *Proc. Natl. Acad. Sci. USA*, **96**, 7910–7915.
Lomize, A.L., Orekhov, V.Y. and Arseniev, A.S. (1992) *Bioorg. Khim.*, **18**, 182–200.
North, C.L. and Cross, T.A. (1995) *Biochemistry*, **34**, 5883–5895.
O'Connell, A.M., Koeppe, R.E.I. and Andersen, O.S. (1990) *Science*, **250**, 1256–1259.
Quine, J.R., Brenneman, M.T. and Cross, T.A. (1997) *Biophys. J.*, **72**, 2342–2348.
Seoh, S.A. and Busath, D.D. (1993) *Biophys. J.*, **65**, 1817–1827.
Smith, S.A., Levante, T.O., Meier, B.H. and Ernst, R.R. (1994) *J. Magn. Reson.*, **A106**, 75–105.
Tian, F. and Cross, T.A. (1999) *J. Mol. Biol.*, **285**, 1993–2003.
Tian, F., Fu, R. and Cross, T.A. (1999) *J. Magn. Reson.*, **139**, 377–381.